Applied Catalysis B: Environmental 136–137 (2013) 239–247

Contents lists available at SciVerse ScienceDirect

Applied Catalysis B: Environmental

journal homepage: www.elsevier.com/locate/apcatb

Catalytic oxidation of toluene by ozone over alumina supported manganese oxides: Effect of catalyst loading

Ebrahim Rezaei[a], Jafar Soltan[a,*], Ning Chen[b,c]

[a] Department of Chemical and Biological Engineering, University of Saskatchewan, 57 Campus Drive, Saskatoon, SK, S7N 5A9, Canada
[b] Canadian Light Source Inc., University of Saskatchewan, 101 Perimeter Road, Saskatoon, SK, S7N 0X4, Canada
[c] Department of Geological Sciences, University of Saskatchewan, 114 Science Place, Saskatoon, SK, S7N 5E2, Canada

ARTICLE INFO

Article history:
Received 26 November 2012
Received in revised form 17 January 2013
Accepted 26 January 2013
Available online 14 February 2013

Keywords:
Toluene
Ozone
Manganese loading
XANES
EXAFS

ABSTRACT

This paper investigates effect of manganese loading on total oxidation of toluene by ozone using alumina-supported manganese oxide catalysts. Activities of four loadings of Mn (1, 5, 10 and 20%) were studied in the temperature range of 22–100 °C. Catalysts were characterized by BET, X-ray diffraction (XRD), X-ray absorption near edge structure (XANES) and extended X-ray absorption fine structure (EXAFS). All catalysts became deactivated at room temperature and their activities were improved by increase of temperature. CHNS and Fourier transform infra red (FT-IR) spectroscopy were used to study catalyst deactivation at room temperature. Alcohols and carboxylic acids were identified as deposited species on the catalysts responsible for catalyst deactivation. A direct relationship between Mn loading and average oxidation state of manganese was found. Catalysts at lower loadings up to 10% were mostly composed of Mn_2O_3 while a mixture of MnO_2 and Mn_2O_3 were present in catalysts with loadings higher than 10%. It was observed that lower Mn loadings have higher activity in oxidation of toluene. It was proposed that lower oxidation states of manganese are more favorable in decomposition of ozone resulting in higher rate of toluene oxidation.

1. Introduction

Catalytic oxidation by ozone is an effective method for low temperature oxidation of volatile organic compounds (VOCs) with a wide variety of application from purification of indoor air to elimination of pollutants in gaseous industrial streams. The main advantage of this method in comparison to catalytic oxidation of VOCs by oxygen is that the required temperature for complete oxidation of pollutants can be reduced by nearly a factor of two leading to energy saving in oxidation processes. Another benefit of catalytic oxidation of VOCs by ozone is use of transition metal oxides which makes it unnecessary to utilize catalysts based on noble metals commonly used in oxidation of VOCs by oxygen. This allows using low cost catalysts for oxidation of VOCs by ozone.

Performance of manganese oxides (MnO_x) dispersed on different supports have been explored for catalytic ozonation of formaldehyde [1], acetone [2,3], cyclohexane [4,5], benzene [6–8] and toluene [9–12]. It can be summarized that the listed VOCs can be oxidized below 100 °C in the presence of ozone and MnO_x. The reason why manganese oxides are of a great catalytic interest is related to their ability in decomposition of ozone. Dhandapani and Oyama showed that MnO_2 is the most active metal oxide among transition metal oxide series for decomposition of ozone [13]. It has been suggested that peroxide and atomic oxygen species generated from decomposition of ozone on MnO_x are responsible for low temperature oxidation of VOCs [2,14].

Even though catalytic ozonation is recognized as an effective method for low temperature oxidation of VOCs, there are challenges related to this method. Deactivation of catalysts at room temperature is one of the main drawbacks of oxidation of VOCs by ozone reported in oxidation of formaldehyde, cyclohexane, benzene and toluene [1,5,6,11]. Zhao et al. showed that catalyst deactivation can be prevented by addition of water vapor to the feed gas resulting in 100% conversion of formaldehyde to CO_2 over a synthesized MnO_x catalyst at room temperature [1]. Einaga and Futamura have reported that water vapor can suppress deactivation of MnO_x/γ-alumina in oxidation of benzene [15]. Einaga et al. have reported that manganese oxides dispersed on ultra stable Y (USY) zeolite can completely oxidize benzene to CO and CO_2 in the presence of water vapor at room temperature [16].

Effect of manganese precursor in catalyst preparation is also important since nitrate and acetate precursors of Mn generate different MnO_x phases on catalysts. The nitrate precursor results in formation of large particles of MnO_2 and Mn_2O_3 [11] while better dispersion of Mn can be attained by using the acetate precursor producing mostly Mn_3O_4 phase [17]. Park et al. examined the effect

* Corresponding author. Tel.: +1 306 966 5449; fax: +1 306 966 4777.
E-mail address: j.soltan@usask.ca (J. Soltan).

0926-3373/$ – see front matter © 2013 Elsevier B.V. All rights reserved.
http://dx.doi.org/10.1016/j.apcatb.2013.01.061

of Mn nitrate and acetate precursors and reported that highly dispersed MnO_x prepared from the acetate precursor show slightly higher activity than the one prepared from the nitrate precursor in catalytic oxidation of benzene by ozone [18,19]. This observation is in agreement with room temperature activities of catalysts reported by Rezaei and Soltan [11].

Catalyst loading is another issue studied by Einaga et al. in catalytic ozonation of benzene over alumina supported manganese oxides [17]. They showed that lower loadings of Mn are more favorable in catalytic ozonation of benzene due to higher dispersion of Mn. On the other hand, Reed et al. reported that higher loadings of Mn on silica are more active in oxidation of acetone by ozone due to their lower oxidation state and higher oxygen delivery ability of adjacent Mn sites in catalysts with higher loadings [3].

This paper investigates the effect of Mn loading in oxidation of toluene over manganese oxides supported on γ-alumina (MnO_x/γ-alumina). This issue has not been thoroughly addressed in the literature. Catalyst activities were studied at room temperature and higher temperatures up to 100 °C. X-ray absorption spectroscopy (XAS) including X-ray absorption near edge structure (XANES) and extended X-ray absorption fine structure (EXAFS) were used to determine electronic and structural properties of the catalysts in order to relate these properties to the observed activities.

2. Experimental

2.1. Catalyst preparation and reference materials

Manganese oxides were dispersed on γ-alumina (Alfa Aesar, S_{BET} = 220 m^2/g) using manganese (II) nitrate tetrahydrate (Sigma–Aldrich, 97%) as the precursor. Catalyst preparation method was dry impregnation and catalysts were denoted as MnO_x/γ-alumina. Four different Mn loadings (1, 5, 10 and 20%) were used to synthesize the catalysts. After impregnation by appropriate amounts of the precursor solution, catalysts were dried at 100 °C for 10 h and calcined at 500 °C for 4 h. The calcined catalysts were crushed and sieved to make particles with diameter less than 208 μm for activity tests.

Mn_2O_3 (Sigma–Aldrich, 99%) and MnO_2 (Alfa Aesar, 99.9%) were used as reference materials in X-ray absorption experiments. X-ray diffraction analysis was performed on the reference materials and bixibytie and pyrolusite were identified as predominant phases of Mn_2O_3 and MnO_2, respectively.

2.2. Catalyst characterization

Brunauer–Emmett–Teller (BET) surface area of the catalysts was determined by nitrogen adsorption at −196 °C using ASAP 2000 (Micromeritics). 0.2 g of the catalysts was degassed at 200 °C for 2 h under vacuum level of 500 μmHga. BET surface area was measured between nitrogen partial pressure ratio (P/P_{atm}) of 0.05 and 0.3. The weight percent of carbon accumulated on the catalysts was measured by CHNS analysis using Vario EL III, Elementar Americans Inc. X-ray diffraction (XRD) was performed on Brucker diffractometer (D8 Advance) using Cu Kα in the 2θ range 10–60° with a step size of 0.04°. Fourier transform infra red (FT-IR) spectra were recorded in the range of 400–4000 cm^{-1} using 32 scans on a JASCO FT/IR 4100 spectrometer with DLATGS detector. The resolution of the detector was 4 cm^{-1}. Samples were diluted with potassium bromide (KBr) and pressed into disks before analysis.

X-ray absorption near edge structure and extended X-ray absorption fine structure of Mn *K-edge* were collected at HXMA beamline, Canadian Light Source (CLS) having a storage ring with 200–250 mA current at 2.9 GeV [20]. The experiments were performed in transmission mode for all samples including the catalysts and the reference materials. The samples were diluted with adequate amount of boron nitride (BN), pressed to thin disks and stuck on Kapton tape in order to obtain an approximately one unit edge jump at the absorption edge. Straight ion chamber detectors were used with Si(1 1 1) monochromator crystal and Rh mirrors as collimating and focusing mirrors, respectively. The scan step-sizes were 10 eV/step, 0.25 eV/step and 0.05 $Å^{-1}$ for the pre-edge, XANES and EXAFS regions, respectively.

2.3. XANES and EXAFS data analysis

Data processing including background removal, data averaging and normalization, energy calibrations and determination of absorption energies were performed by Athena [21]. Absorption energies were obtained based on the position of inflection point in rising part of the spectra. The inflection point was determined by the energy of the major first peak in the 1st derivative of the normalized absorption spectra. EXAFS fitting was performed by Artemis which is a front-end graphical interface for FEFF [22] and IFEFFIT [23]. EXAFS fitting parameters were passive electron reduction factor (S_o^2), coordination number (CN), change in interatomic distance (ΔR), mean-square displacement of the bond length (σ^2) and change in energy scale (ΔE_o). Uncertainties in processing EXAFS data in Artemis were estimated by evaluating the root mean square value of the measured signal in the range of 15–25 Å assuming that no structure can be measured in this range and any signal is due to shot noise [24]. CNs were fixed based on crystallography data of MnO_2 and Mn_2O_3 in EXAFS analysis of the reference materials to obtain S_o^2 which can be used as a fixed parameter in EXAFS analysis of the catalysts. This allows obtaining oxygen and manganese CNs at the first and second shells of MnO_x clusters dispersed on γ-alumina. ΔR, ΔE_o and σ^2 were allowed to be floating for the reference materials and the catalysts and their values were calculated by fitting of EXAFS data.

Unit cell dimensions, space groups [3] and crystal structure of MnO_2 and Mn_2O_3 are shown in Table 1. Basically these are paths which are used for construction of models for fitting of EXAFS data. MnO_2 has originally two oxygen atoms at 1.877 Å and four oxygen atoms at 1.891 Å [3]. But due to their close atomic positions, 6 oxygen atoms at an average distance of 1.887 Å were considered for MnO_2 EXAFS analysis. MnO_2 has one Mn site at the second shell while there are two Mn sites in Mn_2O_3 with occupancy of 25 and 75%. Site 1 with 25% occupancy, has 6 oxygen atoms at 1.993 Å while site 2 has three sets of oxygen atoms at different bond lengths. There are 2 short oxygen bonds at 1.899 Å and two long oxygen bonds at 2.248 Å in site 2. In addition to these 4 oxygen atoms, there are two oxygen atoms at 1.985 Å in site 2 which are extremely close to the oxygen bond length in site 1 at 1.993 Å. The presence of two Mn sites in Mn_2O_3 makes the EXAFS analysis complicated due to close atomic coordinates of oxygen in the two sites. In order to simplify the structure of Mn_2O_3, an averaging method based on the site occupancies was applied to integrate the two Mn sites into one single site for EXAFS analysis. The simplified Mn_2O_3 structure with one site is shown in Table 1. This model was used for EXAFS analysis of the samples containing Mn_2O_3 phase for both the catalysts and Mn_2O_3 reference material.

EXAFS data of the reference materials were fitted simultaneously with *k*-weight of 1, 2 and 3 in order to remove dependency of S_o^2 to different *k*-weights. Catalysts were fitted by *k*-weight of one using sin window function with Δk equal to 1 $Å^{-1}$. The EXAFS data were Fourier transformed in the range of 3–13 $Å^{-1}$ except for the catalyst with Mn loading of 1% which were transformed between 3 and 11 $Å^{-1}$. Data were fitted in *R* space between 0.9 and 3.7 Å for all samples. In all cases the number of variables was kept less than 2/3 of the number of independent points.

Table 1
Crystal structure of reference materials.

MnO_2[a]			Mn_2O_3[b]						Mn_2O_3[c]		
Bond	CN	R_{reff} (Å)[d]	Mn site 1 (25%)			Mn site 2 (75%)			Bond	CN	R_{reff} (Å)[d]
			Bond	CN	R_{reff} (Å)[d]	Bond	CN	R_{reff} (Å)[d]			
Mn—O	6	1.887	Mn—O	6	1.993	Mn—O	2	1.899	Mn—O	1.5	1.899
Mn—Mn	2	2.871	Mn—Mn	6	3.104	Mn—O	2	1.985	Mn—O	3	1.987
Mn—O	4	3.343	Mn—Mn	6	3.565	Mn—O	2	2.248	Mn—O	1.5	2.248
Mn—Mn	8	3.424				Mn—Mn	6	3.115	Mn—Mn	6	3.112
						Mn—Mn	6	3.575	Mn—Mn	6	3.572

[a] Space group: $P\,42/m\,n\,m$, $a = b = 4.396$ Å, $c = 2.871$ Å.
[b] Space group: Ia3, $a = b = c = 9.408$ Å.
[c] Averaged based on Mn site occupancies.
[d] Interatomic distance between neighbors and the absorbing atom obtained from crystallography data.

2.4. Experimental setup and activity tests

The schematic of the experimental set-up is shown in Fig. 1 [11]. Ozone was produced using oxygen (Praxair, 99.993%) by means of an ozone analyzer (AZCO Industries LTD, HTU-500S). The outlet of the ozone generator was mixed with a stream of toluene–nitrogen (Praxair, 300 ppm toluene balanced with nitrogen) to make the feed stream of the reactor. Flow rates of the oxygen–ozone and toluene–nitrogen streams were set at 600 and 400 ml/min, respectively using two Brooks, SLA 5850 mass flow controllers. This arrangement produces 120 and 1050 ppm of toluene and ozone at the inlet of the reactor, respectively. Mole percent of oxygen and nitrogen were 39.94 and 59.94%, respectively. The reactor was made of Pyrex glass located horizontally in an oven (Binder, FP 115) to control the reaction temperature in range of 22–100 °C.

Concentration of ozone was measured by a gas phase ozone analyzer (API 465) while a GC–MS (Agilent, 7890A-5975C) was used for analysis of toluene, CO, CO_2 and other reaction by-products. A capillary column (Varian, Select Permanent Gasses/CO_2, CP7429) was used for CO, CO_2 and toluene measurements while other oxygenated by-products was identified by an Agilent HP-5MS column. More details about the analysis method are available in Ref. [11].

Reaction activity tests were performed on 0.2 g of the catalysts. Total flow rate of the reactants to the reactor was 1000 ml/min resulting in weight hour space velocity (WHSV) of 300 l h^{-1} g^{-1}. Prior to the reaction, toluene, nitrogen and oxygen were passed over the catalyst bed for 1 h while the ozone generator was kept off. After the catalysts became saturated, i.e. outlet concentration of toluene reached the inlet level (120 ppm), the ozone generator was turned on and the oxidation of toluene was monitored at room temperature for 150 min. Immediately after recording the activity of the catalysts at room temperature, the temperature of the oven was increased to 40, 60, 80 and 100 °C in order to obtain activities at higher temperatures. The reaction was monitored for 80 min at each temperature allowing taking two samples for analysis. An averaging method was used to report the activity of the catalysts at 40 and 60 °C since none of the catalysts showed stable activity at these two temperatures. A homogeneous reaction was observed between ozone and toluene during the blank tests using the empty reactor. In order to isolate the heterogeneous reaction contribution of the catalysts, the homogeneous activity was subtracted from the total observed conversions assuming a first order reaction between ozone and toluene in the gas phase. Experiments were repeated and uncertainties in estimation of toluene and ozone conversions were estimated to be 1.5% in terms of standard error.

3. Results and discussion

3.1. Catalyst characterization

BET surface area and pore volume of γ-alumina and the catalysts are shown in Table 2. Monotonic decrease in surface area and pore

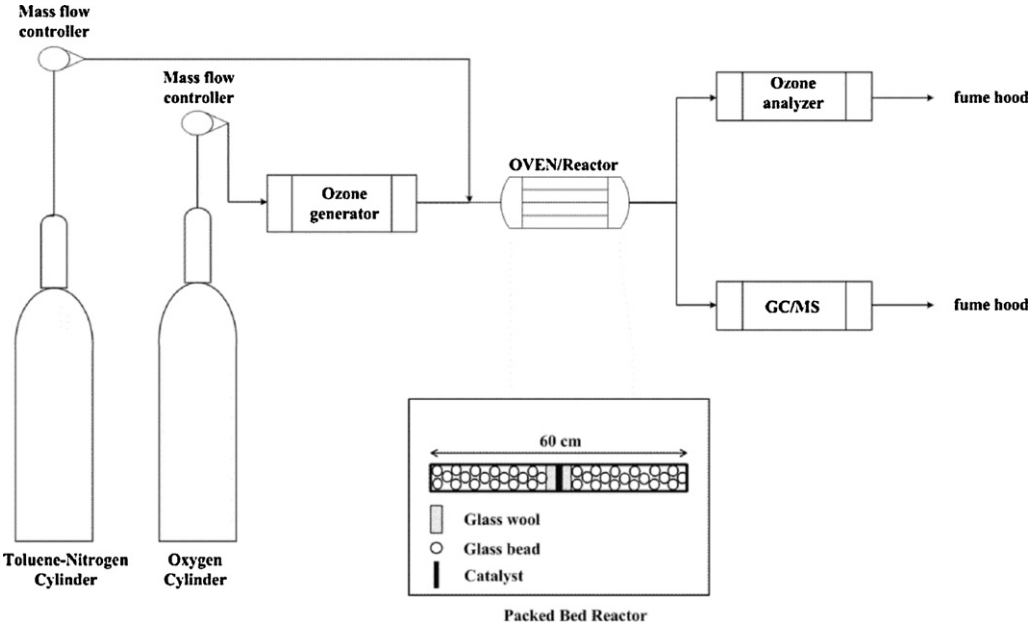

Fig. 1. Schematic of the experimental set-up [11].

Table 2
BET surface area and pore volume of the catalysts.

	γ-alumina	MnO_x/γ-alumina (1%)	MnO_x/γ-alumina (5%)	MnO_x/γ-alumina (10%)	MnO_x/γ-alumina (20%)
BET (m^2/g)	220	217	198	186	164
Pore volume (cm^3/g)	0.61	0.60	0.58	0.51	0.46

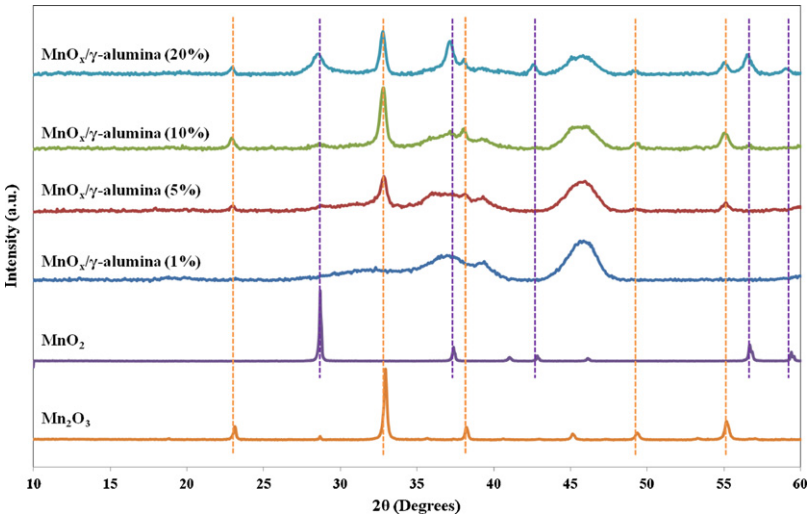

Fig. 2. XRD of reference materials and catalysts.

volume can be seen by increase of loading which can be related to partial plugging of alumina pores.

Fig. 2 shows XRD of the catalysts and the reference materials. Mn_2O_3 has several peaks at 23.1°, 32.9°, 38.2°, 49.3° and 55.2° while MnO_2 peaks are located at 28.7°, 37.3°, 42.8°, 56.7° and 59.4°. These peaks were marked with two dashed lines for Mn_2O_3 and MnO_2 in Fig. 2 in order to track the peak locations on XRD of the catalysts. The catalyst with Mn loading of 1% does not show any diffraction peaks due to high dispersion of manganese oxides on alumina. But MnO_x/γ-alumina (5%) shows peaks matching the spectra of Mn_2O_3. More strong peaks of Mn_2O_3 can be seen in XRD of MnO_x/γ-alumina (10%) along with weak peaks of MnO_2 showing that MnO_2 is coexisting with Mn_2O_3 in this catalyst. With increase of Mn loading to 20%, more intense peaks of MnO_2 are observed while Mn_2O_3 peaks become smaller in XRD spectra of MnO_x/γ-alumina (20%). This shows that with increase of Mn loading, different phases of manganese oxides are formed. At lower loading up to 10%, the dominant phase is Mn_2O_3 while at higher loadings, both MnO_2 and Mn_2O_3 phases coexist.

Mn *K-edge* XANES spectra of the reference materials (MnO_2 and Mn_2O_3) and the catalysts are shown in Fig. 3. It can be seen that the rising part of the spectra of the catalysts with 1 and 5% Mn loading are located at the left side of Mn_2O_3. XANES Spectra of MnO_x/γ-alumina (10%) is closely located at the right side of Mn_2O_3 suggesting that this catalyst is mainly composed of Mn_2O_3. Spectra of the catalyst with 20% are well located between that of Mn_2O_3 and MnO_2 indicating that MnO_x/γ-alumina (20%) has considerable amount of MnO_2 in addition to Mn_2O_3.

Mn *K-edge* absorption energy (E_o) of the reference materials was determined to be 6548.1 and 6552.7 eV for Mn_2O_3 and MnO_2, respectively. Absorption energies of the catalysts are presented in Table 3. MnO_x/γ-alumina (1 and 5%) catalysts have absorption energies less than that of Mn_2O_3 most probably due to the presence of highly dispersed manganese atoms and incomplete growth of Mn_2O_3 unit cells. On the other hand, catalysts with Mn loadings of 10 and 20% have absorption energies higher than that of Mn_2O_3. Absorption energy of MnO_x/γ-alumina (10%) is 0.3 eV higher than E_o of Mn_2O_3 while the sample with 20% Mn has absorption energy at 6552.7 eV which is the same as MnO_2 absorption energy. Linear combination fitting of the catalysts (10 and 20% Mn loading) with the reference materials (MnO_2 and Mn_2O_3) showed that weight percent of MnO_2 increases from 9.0 to 55.3% by increasing Mn loading from 10 to 20%. Meanwhile, fraction of Mn_2O_3 drops from 91.0 to 44.7% from MnO_x/γ-alumina (10%) to MnO_x/γ-alumina (20%). This is in agreement with the XRD results showing that more MnO_2 is formed in MnO_x/γ-alumina by increasing the loading from 10 to 20%.

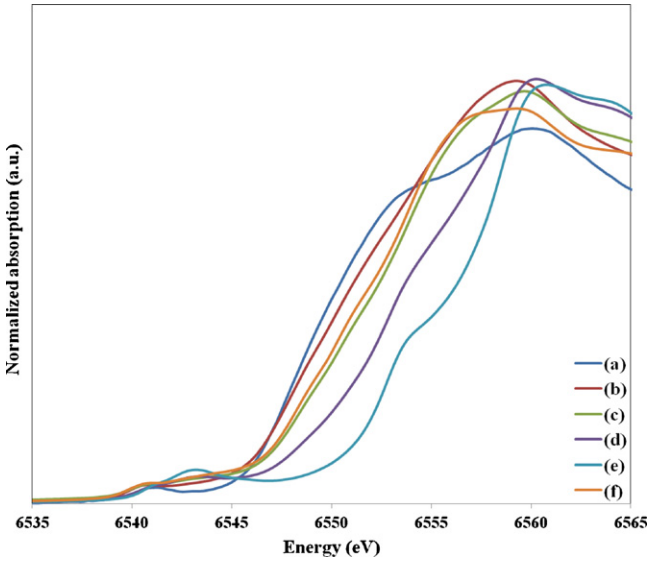

Fig. 3. Mn *K-edge* XANES spectra of the samples, (a) MnO_x/γ-alumina (1%), (b) MnO_x/γ-alumina (5%), (c) MnO_x/γ-alumina (10%), (d) MnO_x/γ-alumina (20%), (e) MnO_2 (f) Mn_2O_3.

Table 3
Mn *K-edge* absorption energies of the catalysts.

	MnO_x/γ-alumina (1%)	MnO_x/γ-alumina (5%)	MnO_x/γ-alumina (10%)	MnO_x/γ-alumina (20%)
Mn *K-edge* E_o (eV)	6547.4	6547.8	6548.4	6552.7

Fig. 4 shows Mn *K-edge* EXAFS oscillation of the samples. The EXAFS spectra of the catalysts with 5 and 10% loading matches the spectra of Mn_2O_3 reference material. On the other hand, EXAFS oscillation of 1% Mn loaded catalyst is different than the spectra of MnO_2 and Mn_2O_3 due to high dispersion of Mn. EXAFS of the catalyst with 20% Mn is similar to the spectra of MnO_2 since the major fraction of manganese oxides in this catalyst is composed of MnO_2.

Using the model explained in Table 1, S_o^2 of MnO_2 and Mn_2O_3 were estimated to be 0.71 ± 0.05 and 0.85 ± 0.06, respectively. The results of the EXAFS fitting of the catalysts are summarized in Table 4. Fig. 5 depicts magnitude and real part of the Fourier transform (FT) of Mn *K-edge* spectra for the catalysts and the fittings. Fig. 5 also contains magnitude and real part of the FT of MnO_2 and Mn_2O_3 in order to provide a guideline for comparison between the catalysts and the reference materials.

Starting with MnO_x/γ-alumina (1%) in Table 4, it can be seen that CN of oxygen and manganese atoms at the first and second shells are smaller than the proposed model for Mn_2O_3 with one single site in Table 1. Low oxygen and manganese CNs can be observed also by noting the magnitude and real part of the FT of MnO_x/γ-alumina (1%) shown in Fig. 5(A.1) and (B.1), respectively. The FT magnitude and real part of the first shell oxygen atoms is smaller than the catalysts with higher loadings in Fig. 5. Mn also shows a very broad weak peak at the second shell of this catalyst (Fig. 5(A.1) and (B.1)) confirming the low CN of manganese.

By increasing the loading to 5%, oxygen CN at ca. 1.99 Å and manganese CN at ca. 3.11 Å increase to 2.1 and 4.2, respectively. Oxygen CNs are basically close to the values considered for Mn_2O_3 in Table 1 (1.5 at 1.899 Å, 3 at 1.987 Å and 1.5 at 2.248 Å) while Mn CN is smaller than 6 which is the expected CN of Mn at the second shell of Mn_2O_3 crystal.

Increase of loading to 10% does not significantly change oxygen CNs while it results in Mn CN of 5.9 which is very close to Mn CN in the second shell of Mn_2O_3. Fig. 5(A.2) and (A.3) also qualitatively show that the intensity of oxygen at the first shell remains unchanged by increasing the loading from 5% to 10% while Mn signal at the second shell shows higher intensity implying higher CN of Mn in MnO_x/γ-alumina (10%) than MnO_x/γ-alumina (5%). It should be noted that the EXAFS of MnO_x/γ-alumina (10%) was modeled based on the structure of Mn_2O_3 and no contribution from MnO_2 was considered in the fitting of this catalyst. This is mainly because of the fact that only 9.0% of MnO_x is in the form of MnO_2 in MnO_x/γ-alumina (10%). This results in the EXAFS oscillation of this catalyst to be similar to that of Mn_2O_3 shown in Fig. 4 allowing fitting EXAFS of MnO_x/γ-alumina (10%) by Mn_2O_3 structure.

In order to model the EXAFS spectra of the catalyst with 20% Mn loading which mostly contains MnO_2 (55.3%), two Mn backscattering atoms from MnO_2 at ca. 2.87 and 3.42 Å were added to the model in order to accommodate contributions of MnO_2. Comparing the common paths (Mn—O at ca. 1.90, 1.99 and 2.25 Å and Mn—Mn at ca. 3.11 Å) in MnO_x/γ-alumina (10%) and MnO_x/γ-alumina (20%), some changes can be seen in coordination numbers due to coexistence of MnO_2 and Mn_2O_3. By increase of Mn loading from 10 to 20%, oxygen CN at ca. 1.90 Å increases from 1.7 to 3.5. On the other hand, oxygen CNs of MnO_x/γ-alumina (20%) at ca. 1.99 and 2.25 Å are 1.1 and 0.9, respectively which are smaller than their corresponding values in MnO_x/γ-alumina (10%), i.e. 2.5 and 1.4 at ca. 1.99 and 2.25 Å, respectively. CN of Mn at ca. 3.11 decreases from 5.9 in MnO_x/γ-alumina (10%) to 2.1 in MnO_x/γ-alumina (20%). In addition to these changes, two new manganese atoms were resolved at ca.

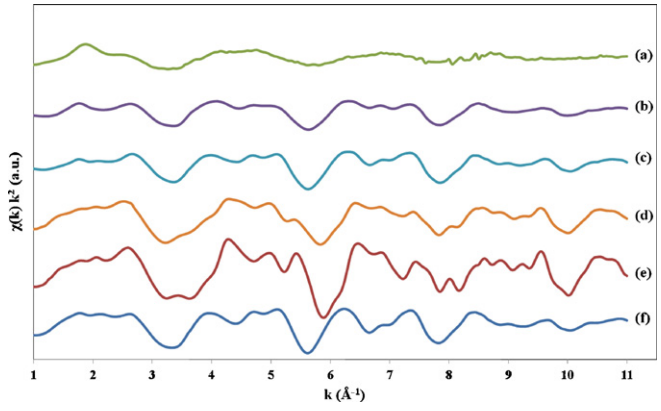

Fig. 4. Mn *K-edge* EXAFS spectra of the samples, (a) MnO_x/γ-alumina (1%), (b) MnO_x/γ-alumina (5%), (c) MnO_x/γ-alumina (10%), (d) MnO_x/γ-alumina (20%), (e) MnO_2, (f) Mn_2O_3.

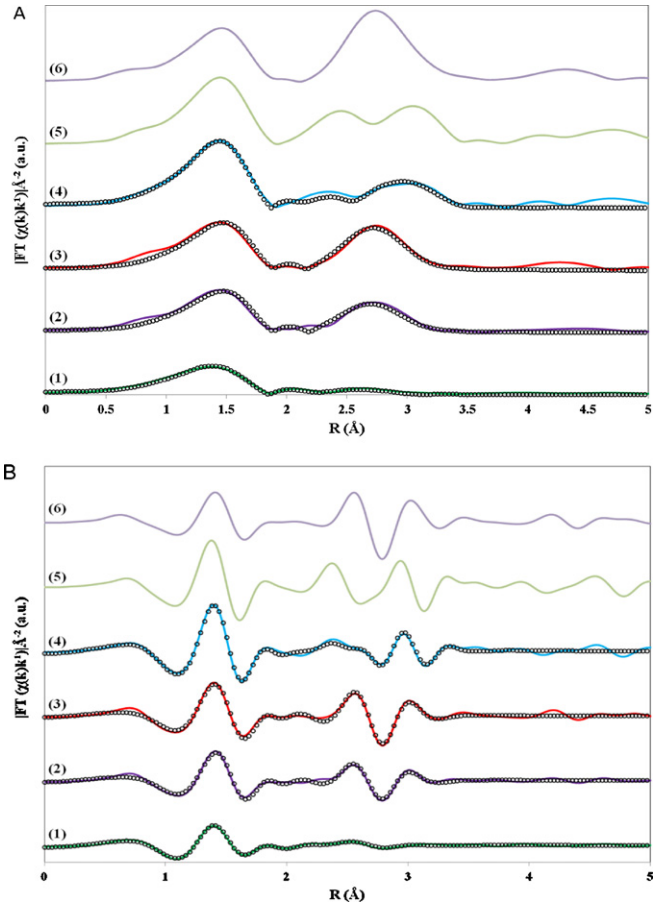

Fig. 5. Magnitude (A) and real part (B) of the Fourier transform of Mn *K-edge* data (solid lines) and fitting (symbols), (1) MnO_x/γ-alumina (1%), (2) MnO_x/γ-alumina (5%), (3) MnO_x/γ-alumina (10%), (4) MnO_x/γ-alumina (20%), (5) MnO_2, (6) Mn_2O_3.

Table 4
EXAFS fitting results of the catalysts.

	Path	CN	σ^2 ($\times 10^{-3}$ Å^2)	R (Å)	E_o (eV)	R_f (%)[a]
MnO_x/γ-alumina (1%)	Mn—O	1.7 ± 0.5	7.0 ± 1.6	1.886 ± 0.017	0.2 ± 1.6	0.9
	Mn—O	1.2 ± 0.2		1.985 ± 0.017		
	Mn—O	1.4 ± 0.3		2.236 ± 0.017		
	Mn—Mn	1.0 ± 0.5	17.4 ± 9.3	3.105 ± 0.026		
MnO_x/γ-alumina (5%)	Mn—O	1.7 ± 0.6	5.4 ± 1.8	1.904 ± 0.018	4.5 ± 1.1	2.4
	Mn—O	2.1 ± 0.5		1.990 ± 0.018		
	Mn—O	1.4 ± 0.1		2.254 ± 0.018		
	Mn—Mn	4.2 ± 1.2	10.5 ± 3.0	3.117 ± 0.014		
MnO_x/γ-alumina (10%)	Mn—O	1.7 ± 0.4	4.6 ± 1.6	1.894 ± 0.015	5.0 ± 0.9	1.6
	Mn—O	2.5 ± 0.5		1.985 ± 0.015		
	Mn—O	1.4 ± 0.1		2.249 ± 0.015		
	Mn—Mn	5.9 ± 1.1	9.6 ± 1.9	3.127 ± 0.011		
MnO_x/γ-alumina (20%)	Mn—O	3.5 ± 0.5	3.3 ± 1.3	1.884 ± 0.009	0.17 ± 1.4	1.5
	Mn—O	1.1 ± 0.1		1.970 ± 0.009		
	Mn—O	0.9 ± 0.1		2.234 ± 0.009		
	Mn—Mn	1.4 ± 0.2	4.7 ± 1.2	2.882 ± 0.012		
	Mn—Mn	2.1 ± 0.1		3.115 ± 0.012		
	Mn—Mn	4.0 ± 0.3		3.435 ± 0.012		

[a] The absolute percentage misfit between theory and data [24].

2.88 Å and 3.44 Å with CN of 1.4 and 4.0 which are the coordinates of manganese atoms in the structure of MnO_2.

If one makes an average over oxygen and manganese CNs based on weight percent of MnO_2 (55.3%) and Mn_2O_3 (44.7%) in MnO_x/γ-alumina (20%) and uses CNs available in Table 1 for MnO_2 and Mn_2O_3 (with one single Mn site), a simplified model can be obtained for the catalysts with 20% Mn loading which is shown in Table 5. Based on this approach, one would expect 4.0, 1.4 and 0.7 oxygen atoms at ca. 1.90, 1.99 and 2.25 Å, respectively. In addition, this method results in 1.1, 2.7 and 4.4 of manganese atoms at ca. 2.87, 3.11 and 3.42 Å, respectively. It can be seen that the result of EXAFS fitting of MnO_x/γ-alumina (20%) reported in Table 4, follows the trend of CN changes shown in Table 5 implying that EXAFS fitting results are fairly reasonable.

R factors (R_f) reported in Table 4 represent absolute percentage misfit between data and theory. All fittings show low R_f values around 2% which shows that the models have been fitted closely to the EXAFS data. It is important to note that fitting results with *k*-weights of 2 and 3 were consistent with the results of Table 4 using *k*-weight of 1. But the lowest *R* factors (best fits) were obtained with *k*-weight of 1 reported in Table 4.

3.2. Oxidation of toluene by ozone

Four loadings of Mn (1, 5, 10 and 20%) were used for oxidation of toluene by ozone at room temperature and higher temperatures up to 100 °C. Toluene and ozone conversion at room temperature are indicated in Fig. 6(A) and (B) respectively. It can be seen that the activity of the catalysts decreases with increases of Mn loading. MnO_x/γ-alumina (1%) shows the highest activity followed by catalysts with 5, 10 and 20% loadings. CO_x (CO and CO_2) were detected as the major by-product of the reaction but the selectivity of the oxidation reaction to CO_x was only around 20% at room temperature. All catalysts lost their activity during the reaction course in terms of toluene and ozone conversions showing that deactivation of the catalysts occurs at room temperature. CHNS analysis was performed on the catalysts after running the reaction

Table 5
Averaged coordination numbers of MnO_x/γ-alumina (20%).

Path	R_{reff} (Å)	Coordination number (CN)
Mn—O	1.892	4.0
Mn—O	1.987	1.4
Mn—O	2.248	0.7
Mn—Mn	2.871	1.1
Mn—Mn	3.112	2.7
Mn—Mn	3.424	4.4

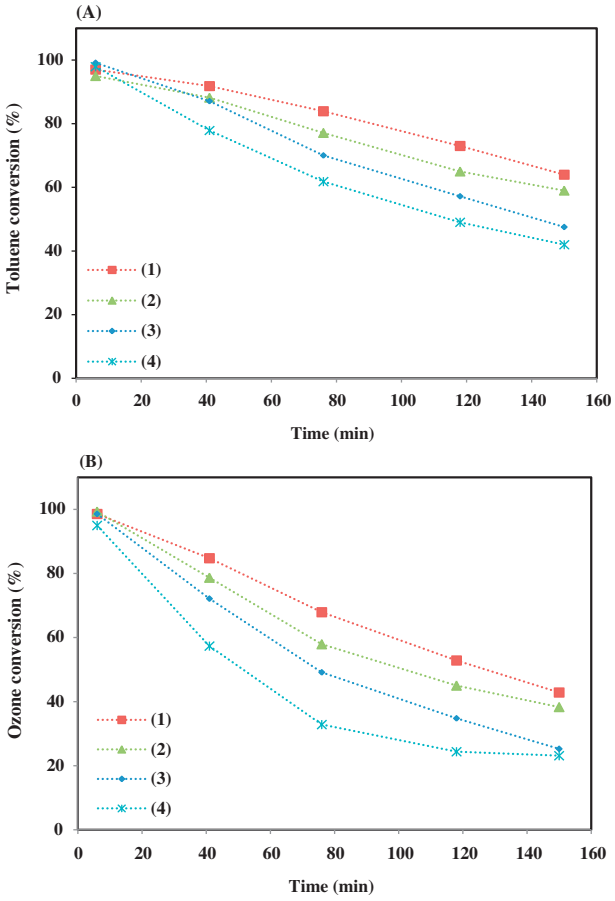

Fig. 6. Room temperature activity of the catalysts, (A) toluene conversion, (B) ozone conversion, (1) MnO_x/γ-alumina (1%), (2) MnO_x/γ-alumina (5%), (3) MnO_x/γ-alumina (10%), (4) MnO_x/γ-alumina (20%).

Table 6
Accumulated carbon content on the catalysts after 150 min reaction at room temperature.

	MnO_x/γ-alumina (1%)	MnO_x/γ-alumina (5%)	MnO_x/γ-alumina (10%)	MnO_x/γ-alumina (20%)
Carbon content (wt%)	11.16	11.01	10.25	9.00

for 150 min at room temperature in order to measure deposited carbon content of the catalysts. The results, shown in Table 6, indicate that all the four catalysts gain considerable amount of carbon which can be considered as the reason for catalyst deactivation. Low selectivity of the reaction to CO_x and presence of carbonaceous species on the catalysts suggest that partial oxidation of toluene occurs at room temperature resulting in accumulation of carbon containing compounds on the catalysts. Table 6 also shows that the most active catalyst, MnO_x/γ-alumina (1%), gains higher carbon content than the other catalysts. The amount of accumulated carbon decreases with increase of Mn loading in all catalysts. This trend can be explained with respect to the fact that the nature of the ongoing reaction at room temperature is mostly partial oxidation of toluene to carbonaceous compounds depositing on the catalysts. Therefore, MnO_x/γ-alumina (1%) with the highest activity among the catalysts only partially oxidizes more toluene to deposited carbonaceous species and not necessarily to higher amount of CO and CO_2 in comparison to the catalysts with higher Mn loadings. The same discussion can be applied to the catalysts with 5, 10 and 20% Mn loadings justifying why deposited carbon content of the catalysts reduces with increase of Mn loading at room temperature.

FT-IR spectra of fresh γ-alumina and the catalysts after 150 min of reaction at room temperature are shown in Fig. 7. Spectra of fresh γ-alumina not used in the reactor, Fig. 7(a), show peaks at 1622, 2350 cm^{-1} and a broad signal between 2500 and 3800 cm^{-1} which are due to adsorbed water and CO_2 and hydroxyl groups on alumina, respectively. All four catalysts show new bands at 1410, 1718 cm^{-1} which are indicative of C—O—H bending of alcohols and carbonyl group (C=O) stretch of carboxylic acids, respectively [25]. In addition, a broad peak in the range 2500–3800 cm^{-1} is observed on all catalysts which can be due to overlapping of OH stretching of carboxylic acids and alcohols with that of adsorbed water [6]. The intensity of these new peaks (1410, 1718 and 2500–3800 cm^{-1}) becomes smaller with increase of Mn loading implying that the amount of deposited alcohols and carboxylic acids decrease with increase of manganese loading. This is also qualitatively in agreement with the result of CHNS analysis suggesting that the order of carbon content of the used catalysts has reverse relationship with Mn loading. Einaga and Futamura reported formic acid, 2,5-furandione, phenol, acetic acid and oxalic acid as the accumulated compounds on MnO_x/γ-alumina after oxidation of benzene with ozone at room temperature [6]. We have also identified acetic acid and oxalic acid, benzene and maleic anhydride as the minor by-products of the reaction by monitoring the reaction at 80 °C [11]. Presence of acetic acid and oxalic acid also supports identification of carboxylic acids on the catalysts at room temperature due to incomplete oxidation of toluene.

Results of high temperature activity of the catalysts up to 80 °C are shown in Fig. 8. Activity orders are similar to the room temperature activities indicating that lower Mn loadings result in higher conversion of toluene and ozone. It can be seen that increase of temperature from room temperature (22 °C) enhances toluene and ozone conversions up to 80 °C. All the four catalysts show the same activity at 80 °C at which, maximum conversion of toluene occurs. Increase of temperature from 80 to 100 °C (data not shown) decreases toluene conversion to some extent while the conversion of ozone remains constant at 100%. As mentioned before, acetic acid, oxalic acid, benzene and maleic anhydride were minor by-products of the reaction while the main reaction by-products were

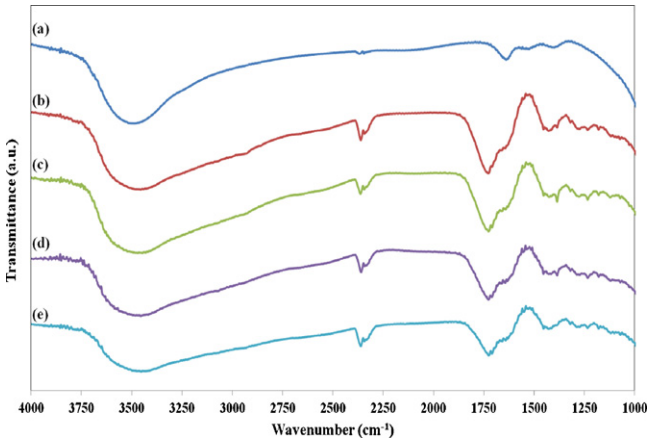

Fig. 7. FT-IR spectra of the deactivated catalysts after 150 min reaction at room temperature, (a) fresh γ-alumina, (b) MnO_x/γ-alumina (1%), (c) MnO_x/γ-alumina (5%), (d) MnO_x/γ-alumina (10%), (e) MnO_x/γ-alumina (20%).

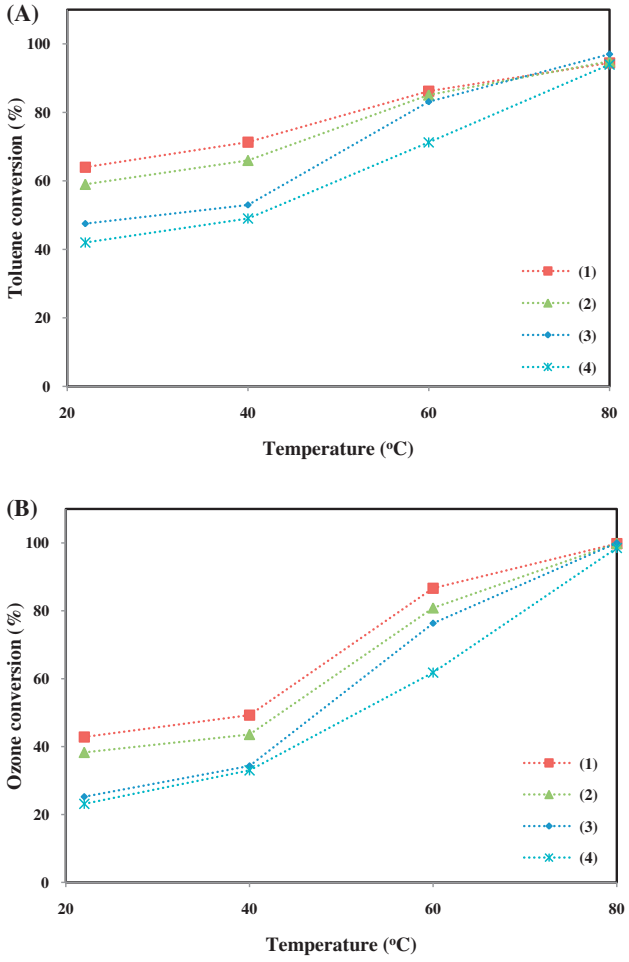

Fig. 8. Activity of the catalysts as a function of temperature, (A) toluene conversion, (B) ozone conversion, (1) MnO_x/γ-alumina (1%), (2) MnO_x/γ-alumina (5%), (3) MnO_x/γ-alumina (10%), (4) MnO_x/γ-alumina (20%).

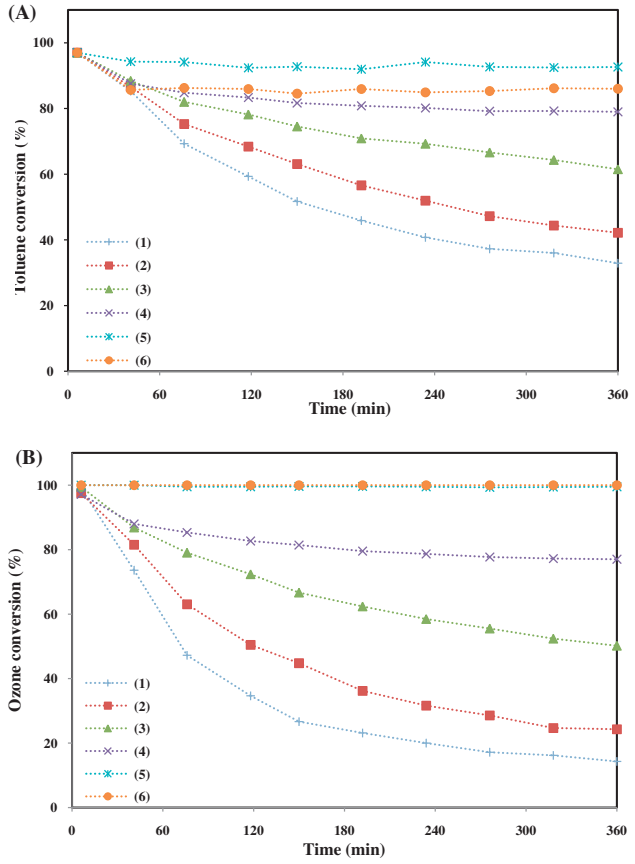

Fig. 9. Long term activity of MnO_x/γ-alumina (10%) at different temperatures, (A) toluene conversion, (B) ozone conversion, (1) 22 °C, (2) 40 °C, (3) 55 °C, (4) 65 °C, (5) 80 °C, (6) 100 °C.

CO and CO_2 at all temperatures with maximum selectivity to CO_x of around 90% at 80 °C. Long term activities were also studied on MnO_x/γ-alumina (10%) in order to find the minimum temperature at which, no catalyst deactivation occurs. Toluene and ozone conversions were monitored at 22, 40, 55, 65, 80 and 100 °C for 6 h at each temperature and the results are shown in Fig. 9. It was observed that 65 °C (Fig. 9(A.4) and (B.4)) is the minimum temperature that the catalysts function without deactivation. Maximum toluene conversion was around 95% which was obtained at 80 °C. A decrease in toluene conversion can be seen by increasing temperature from 80 to 100 °C. One possible reason for this observation is that all ozone is already consumed at 80 °C and increase of temperature from 80 to 100 °C accelerates decomposition of ozone resulting in less available surface oxygen species to take part in toluene oxidation reaction.

The overall observation of the activities at room and higher temperatures suggests that catalysts with lower loadings of Mn are more active for oxidation of toluene by ozone. Einaga et al. have studied effect of Mn loading in oxidation of benzene by ozone at room temperature over MnO_x/γ-alumina [17]. They reported that catalysts with lower loadings (1–7.5%) have slightly higher activities and isolated Mn atoms in lower loadings and aggregated Mn_3O_4 clusters in higher loadings (10–15%) show almost similar activities. On the other hand, Reed et al. have showed that higher loadings of Mn on silica result in higher oxidation rate of acetone by ozone [3]. They proposed that lower oxidation state of Mn and more adjacent Mn sites in catalysts with higher Mn loadings are two factors controlling the rate of acetone oxidation by ozone. They have also mentioned that the rate controlling step of acetone ozonation is oxidation of the catalyst by ozone and not the oxidation of acetone by the catalyst. The mechanism of oxidation of VOCs by ozone is based on ozone decomposition due to Eqs. (1)–(3) generating atomic oxygen to react with VOCs in the oxidation reaction (Eq. (5)) assuming that VOCs are adsorbed on Mn sites (Eq. (4)) and the reaction proceeds based on Langmuir–Hinshelwood mechanism between adsorbed species (Eq. (5)) [14,26,27]:

$$O_3 + Mn \rightarrow O_2 + O{-}Mn \quad (1)$$

$$O_3 + O{-}Mn \rightarrow O_2 + O_2{-}Mn \quad (2)$$

$$O_2{-}Mn \rightarrow O_2 + Mn \quad (3)$$

$$VOC + Mn \rightarrow VOC{-}Mn \quad (4)$$

$$VOC{-}Mn + O{-}Mn \rightarrow Products \quad (5)$$

It is believed that higher dispersion of Mn atoms in catalysts with lower loading levels decreases oxidation state of Mn. As oxidation state of Mn decreases, the ability of Mn atoms in transferring electrons to ozone in Eq. (1) ($O_3 + Mn^{n+} \rightarrow O_2 + O^{2-} + Mn^{(n+2)+}$) increases causing faster decomposition rate of ozone to atomic oxygen and consequently higher rate of toluene oxidation. In fact, activity orders of the catalysts can be related to the reverse of Mn *K-edge* absorption energy orders reported in Table 3. Einaga and Ogata also found that higher dispersion of Mn is more effective in benzene ozonation at room temperature [8] but it seems that changes in Mn oxidation state as the result of variation in Mn dispersion is controlling the rate of oxidation of aromatics such as benzene and toluene by ozone.

4. Conclusion

Effect of Mn loading on activity of alumina supported manganese oxide catalysts were studied in the temperature range of 22–100 °C. Characterization of the catalysts by XRD, XANES and EXAFS analysis showed that Mn_2O_3 is the dominant phase at lower catalyst loadings; whereas mixture of MnO_2 and Mn_2O_3 was observed at higher catalyst loadings. Fraction of MnO_2 and oxidation state of Mn increased with increase of Mn loading. It was shown that lower Mn loadings are more favorable in oxidation of toluene up to 80 °C at which, the catalysts show the same activity. All catalysts became deactivated at room temperature due to accumulation of alcohols and carboxylic acids on the surface of the catalysts indicated by CHNS and FT-IR analyses. It was suggested that activity orders of the catalysts are related to the oxidation state of Mn on the catalyst. Catalysts with lower Mn loadings have higher activity in transferring electrons to ozone to initiate ozone decomposition reaction due to their lower oxidation state. This increases rate of decomposition of ozone to atomic oxygen which consequently enhances oxidation rate of toluene.

Acknowledgments

Authors gratefully acknowledge the University of Saskatchewan and the Natural Sciences and Engineering Research Council of Canada (NSERC) for their financial support provided for this research. XAS experiments were performed at the Canadian Light Source (CLS), which is supported by the NSERC, the National Research Council Canada, the Canadian Institutes of Health Research, the Province of Saskatchewan and Western Economic Diversification Canada.

We also would like to thank XAFS.ORG and Ifeffit Mailing list community for providing valuable information about XAS data processing and analysis.

References

[1] D. Zhao, C. Shi, X. Li, A. Zhu, B.W. Jang, Journal of Hazardous Materials 239–240 (2012) 362–369.
[2] Y. Xi, C. Reed, Y.-K. Lee, S.T. Oyama, Journal of Physical Chemistry B 109 (2005) 17587–17596.
[3] C. Reed, Y.-K. Lee, S.T. Oyama, Journal of Physical Chemistry B 110 (2006) 4207–4216.
[4] H. Einaga, S. Futamura, Reaction Kinetics and Catalysis Letters 81 (2004) 121–128.
[5] H. Einaga, S. Futamura, Applied Catalysis B 60 (2005) 49–55.
[6] H. Einaga, S. Futamura, Journal of Catalysis 227 (2004) 304–312.
[7] H. Einaga, S. Futamura, Catalysis Communications 8 (2007) 557–560.
[8] H. Einaga, A. Ogata, Journal of Hazardous Materials 164 (2009) 1236–1241.
[9] M. Sugasawa, A. Ogata, Ozone: Science and Engineering 33 (2011) 158–163.
[10] E. Park, S. Chin, J. Kim, G.-N. Bae, J. Jurng, Powder Technology 208 (2011) 740–743.
[11] E. Rezaei, J. Soltan, Chemical Engineering Journal 198–199 (2012) 482–490.
[12] M. Li, K.N. Hui, K.S. Hui, S.K. Lee, Y.R. Cho, H. Lee, W. Zhou, S. Cho, C.Y.H. Chao, Y. Li, Applied Catalysis B 107 (2011) 245–252.
[13] B. Dhandapani, S.T. Oyama, Applied Catalysis B 11 (1997) 129–166.
[14] C. Reed, Y. Xi, S.T. Oyama, Journal of Catalysis 235 (2005) 378–392.
[15] H. Einaga, S. Futamura, Journal of Catalysis 243 (2006) 446–450.
[16] H. Einaga, Y. Teraoka, A. Ogat, Catalysis Today 164 (2011) 571–574.
[17] H. Einaga, M. Harada, A. Ogata, Catalysis Letters 129 (2009) 422–427.
[18] J.H. Park, J.M. Kim, M. Jin, J.K. Jeon, S.S. Kim, S.H. Park, S.C. Kim, Y.K. Park, Nanoscale Research Letters 7 (2012) 2–5.
[19] J.H. Park, J. Jurng, G.N. Bae, S.H. Park, J.K. Jeon, S.C. Kim, J.M. Kim, Y.K. Park, Journal of Nanoscience and Nanothecnology 12 (2012) 5942–5946.
[20] D.T. Jiang, N. Chen, W. Sheng, AIP Conference Proceedings 879 (2007) 800–803.
[21] B. Ravel, M. Newville, Journal of Synchrotron Radiation 12 (2005) 537–541.
[22] J.J. Rehr, R.C. Alber, Reviews of Modern Physics 72 (2000) 621–654.
[23] M. Newville, Journal of Synchrotron Radiation 8 (2001) 322–324.
[24] B. Ravel, EXAFS Analysis with FEFF and FEFFIT, Part 2: Commentary, 2001.
[25] D.L. Pavia, G.M. Lampman, G.S. Kriz, J.R. Vyvyan, Introduction to Spectroscopy, fourth ed., Brooks/Cole, Cengage Learning, 2009.
[26] R. Radhakrishnan, S.T. Oyama, J.G. Chen, K. Asakura, Journal of Physical Chemistry B 105 (2001) 4245–4253.
[27] R. Radhakrishnan, S.T. Oyama, Journal of Catalysis 199 (2001) 282–290.